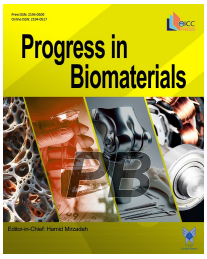

Volume 13, Issue 2, 132408 (1-10)

Progress in Biomaterials (PIBM)

https://doi.org/10.57647/pibm.2024.132408

Feasibility Study of Streptozotocin (STZ) Induced Cellular Changes Using Tamm Plasmon Polaritons in a One-Dimensional Photonic Crystal

Mitra Bahrami, Seyedeh Mehri Hamidi*

Magneto-plasmonic Lab, Laser and Plasma research Institute, Shahid Beheshti University, Tehran, Iran.

***Corresponding author:** m_hamidi@sbu.ac.ir

Original Research

Abstract:

In this research, we design, simulate, and validate a label-free optical sensor that we use to monitor STZ-induced changes in neural stem cells. The basis of this sensor is the tamm plasmon polariton (TPP), which is excited at the interface of a one-dimensional photonic crystal and a thin layer of gold. In this work, we optimize the thickness of the gold layer and the measurement method by simulation based on the transfer matrix to increase the sensitivity of the sensor. After making the designed sensor, we cultured third-pass neural stem cells from the hippocampus of neonatal Wistar rats on it. After treating the cells with STZ, known to induce Alzheimer-like changes *in vitro*, the reflection spectra were recorded at selected time points (0, 17, and 30 h), illustrating the sensor's potential for real-time monitoring of cellular responses. Finally, we compared and analyzed the simulation and experimental results. The proposed sensor, as a non-invasive, high-sensitivity, and real-time method, can be used to monitor Alzheimer's-like processes in laboratory conditions.

Keywords:

Tamm surface waves; Photonic crystal; Streptozotocin; Sensor; Alzheimer disease; Magneto-plasmonic

Cite this article: Bahrami, M., Hamidi, S. M. Feasibility Study of Streptozotocin (STZ) Induced Cellular Changes Using Tamm Plasmon Polaritons in a One-Dimensional Photonic Crystal. *Progress in Biomaterials* **13**(2), Article 08 (2024).

1. Introduction

Optical biosensors based on surface electromagnetic states enable label-free and real-time detection. For example, surface plasmon waves (SPWs) are electromagnetic modes that form at the metal-dielectric interface. These waves have been widely employed in sensing applications. One of the limitations of this method is that it is excited only in transverse magnetic polarization (TM). On the other hand, to excite these waves, phase-matching techniques and coupling elements such as prisms and gratings are needed (Homola and Piliarik, 2006; Maier, 2007; Polo Jr and Lakhtakia, 2011). In contrast, Bloch surface waves (BSWs) that propagate at the boundary of a one-dimensional photonic crystal and a dielectric medium can be excited under both transverse electric (TE) and TM polarizations (Konopsky and Alieva, 2007). In one-dimensional photonic crystals, the periodicity of the refractive index creates photonic band gaps, which enable the encapsulation of BSWs. This confinement results in resonance characteristics that are very sensitive to changes in the refractive index of the surrounding environment, and this sensitivity becomes the basis of sensing in this method (Morozov et al., 2006; Danz et al., 2012; Sinibaldi et al., 2012). On the other hand, these sensors have mechanical strength and stability in environments due to their dielectric structure. Nonetheless, BSWs also require coupling elements for excitation.

Because BSWs and SPWs cannot be excited with free-space light, researchers looked for alternative methods. For this purpose, TPPs provide an experimentally demonstrated and practical solution. Unlike surface plasmon resonances (SPR) that are only excited by waves with TM polarization, TPPs are excited by both polarizations (Gryga et al., 2020; Kavokin et al., 2005). This feature eliminates the need for additional components in SPR sensors, thereby simplifying the system. On the other hand, unlike BSWs and SPWs, these waves do not need coupling elements and are also excited by free-space light, which also leads to a simpler sensing system.

In 1932, Tamm first proposed the concept of localized electronic states on crystal surfaces and established the theoretical foundations of surface phenomena. Based on this, in

2007, Kaliteevski et al. predicted the existence of optical states of TPP. As mentioned, TPPs are surface electromagnetic states that arise at the common boundary of a Bragg reflector and a metal layer. The following year, Sasin et al. demonstrated TPPs experimentally. They showed that these waves can support slow light propagation with strong spatial limitation (Kaliteevski et al., 2007; Tamm, 1932; Sasin et al., 2008). Recent studies have shown that these waves have significant potential in sensor applications. TPPs have significant applications in various fields such as optical switching (Lee et al., 2013; Bessonov et al., 2017), solar cells (Pykhtin et al., 2024; Bikbaev et al., 2021), filters (Chen, 2020; Normani et al., 2022) and perfect absorbers (Xue et al., 2016; Gong et al., 2011; Orojloo et al., 2024). We are looking to design a TPP sensor to aid our in Alzheimer's vitro research in neural culture models.

Alzheimer's disease is a progressive neurological disorder that affects millions of people worldwide. This disease is mostly associated with cognitive disorders, memory loss, and neuronal dysfunction. Pathological features of Alzheimer's include deposition of extracellular amyloid-□ (A□) plaques (Lei, 2010), excessive phosphorylation of tau in cells (Paula et al., 2009), loss of synapses (Serrano-Pozo et al., 2011), and neuroinflammation (Serrano-Pozo et al., 2011). Because the disease is progressive, early detection of Alzheimer's is very important (Ahmad et al., 2023). In fact, treatments in the early stages of the disease have the greatest potential to reduce the speed of disease progression and preserve cognitive functions. Laboratory studies using neural culture models are employed to investigate treatments and understand biomolecular interactions (Schlachetzki et al., 2013). But conventional measurement methods in these models only provide endpoint information and cannot provide cellular pathology at any moment. This limitation further emphasizes the need for a biosensor that can dynamically monitor neuronal health and Alzheimer's-related biomarkers in a label-free manner. In this study, we use STZ to induce Alzheimer-like effects in neural cells.

Streptozotocin (STZ) is a nitrosourea compound that is widely used to induce diabetes in animal models. It has also recently been used in cell models of Alzheimer's disease. STZ inhibits the phosphorylation of the insulin receptor substrate (IRS) and prevents the activation of PI3K and the subsequent production of PIP3. Finally, inactivation of Akt reduces GLUT2 translocation to the plasma membrane and impairs glucose uptake in neurons. Subsequently, intracellular Ca^{2+} accumulation and reactive oxygen species (ROS) production increase, leading to the release of inflammatory cytokines and contributing to the neurodegenerative processes characteristic of Alzheimer's disease (Figure 1a) (Crunfli et al., 2018).

In Alzheimer's disease research, to determine the effectiveness of therapeutic interventions, it is necessary to monitor the effect of STZ on cells at every moment (Crunfli et al., 2018). So far, no study has investigated Alzheimer-like cellular processes using TPPs. Addressing this gap can provide a non-destructive, real-time sensing method without the limitations of existing optical approaches for Alzheimer's disease modeling.

For Alzheimer's studies, we need biosensors that can monitor cell activity in real time without labels. Traditional biochemical analyses, such as Western blot (Kulichikhin et al., 2021), ELISA (Hsiao et al., 2023), and immunofluorescence (Park et al., 2019) are superior in terms of measuring the presence of A□, tau hyperphosphorylation, and neurotoxicity, but they only provide endpoint information and are destructive. This limitation has led to interest in label-free optical methods that have the ability to make high-sensitivity measurements in living cells in real time.

Significant progress has been made in optical biosensing for Alzheimer's disease, but the methods available *in vitro* studies have weaknesses. The FRET optical technique can track the accumulation of amyloid beta and tau protein in real time, but this method requires genetic labeling of proteins with fluorophores, and fluorophores are gradually photobleached (Lathuiliere et al., 2023). In new research, SPR sensors have been modified so that they can also investigate the behavior of living cells (Gheorghiu et al., 2014). For example, by combining SPR and electrical impedance spectroscopy (EIS), it is possible to see what effect amyloid proteins have on living cells in culture (Zeidan et al., 2015). This method provides the possibility of measuring the physical interactions of the cell culture environment. Raman and SERS can be used for label-free imaging, but both methods have disadvantages (Gu et al., 2020; Elsheikh et al., 2024). Nano-biosensors are highly sensitive, but most cannot provide real-time measurements or require additional materials such as labels (Singh et al., 2023). New photonic crystal-based and phase sensors can detect subtle cellular changes label-free and in real time; however, their performance on STZ-treated neurons has not yet been evaluated. The STZ model is one of the most commonly used in vitro models for studying Alzheimer-like cellular changes (Chen et al., 2013; Li et al., 2023).

By addressing this gap, we can provide a tool to monitor Alzheimer-like cellular changes in real time in a non-destructive manner, which can aid in elucidating disease mechanisms and evaluating potential therapeutics. In TPP platforms, a very strong and concentrated electromagnetic field is created, and optical losses are minimal, which results in high sensitivity, enabling label-free detection of neuronal biomarkers and subtle changes in the culture medium. TPPs are formed at the interface between a one-dimensional photonic crystal and a thin metal layer and have properties of strong surface-based field confinement and low optical loss, as well as excitation at normal incidence. Excitation of TPPs at normal incidence allows for simpler and more stable sensor designs (Gupta and Nair, 2015). But despite these properties, this method has not yet been investigated for Alzheimer's pathology in nerve cell cultures.

TPPs were first observed experimentally at the interface of a Bragg mirror and a thin metal layer (Kaliteevski et al., 2007), and then showed excitation at normal incidence, which is an advantage over conventional surface plasmon polaritons (SPPs) (Sasin et al., 2008). By engineering and optimizing Bragg dielectric stacks and metal layers, the TPPs can be changed. In fact, by adjusting the thickness of the metal layer and the dielectric layer, the localization

of the field increases, and the resonances can be adjusted. Therefore, by precisely engineering the layers, highly sensitive and tunable sensors (Chang et al., 2014).

Structural optimization has been used to enhance the performance of TPP sensors in recent reports. Du et al. (2019) reported that introducing a defect layer in TPP sensor structures produced an exceptional sensitivity of 416 nm/RIU and a figure of merit (FOM) of 682 RIU^{-1}, due to the formation of an electromagnetically induced transparency-like effect that generates ultranarrow spectral peaks (Du et al., 2019). In 2017, Huang et al. investigated the phase-sensitive detection mode. They achieved a high sensitivity of approximately $\sim 2 \times 10^5$ °/RIU of p and s polarized light in optimized TPP sensors (Huang et al., 2017). In 2021, Das et al. worked out a hybrid Tamm-Fabry-Perot resonance sensor. These sensors were created by the use of subwavelength metal gratings and were able to show sensitivity up to 160 nm/RIU with FOM of about 7.5 RIU^{-1} (Das et al., 2021). In 2024, Haidar et al. demonstrated the incorporation of porous layers between metal nanostructures. They have also dispersed Bragg reflectors that could be used to increase sensitivity as high as 40 nm/RIU to 200 nm/RIU, a fivefold betterment when material engineering is properly applied (Haidar et al., 2024).

On the other hand, recent research, TPP sensors in biological applications has also made significant progress in highly sensitive and label-free detection. Rong and Sawan in 2023 produced a TPP-based biosensor of porous silicon with a high sensitivity of 1.5 nm/(μg/mL) and detection limits of 7 ng/mL in detecting the nucleocapsid protein of SARS-CoV-2 (Rong and Sawan, 2023). Su et al. in 2023 improved the TPP biosensor performance by using one-dimensional topological photonic crystals, which achieved a notable sensitivity of 2.6553×10^4 RIU^{-1} in TM-polarization mode, and the value of the figure of merit 3.1238×10^7 $RIU^{-1}deg^{-1}$ and was polarization-independent and tolerable to fabrication changes (Su et al., 2023). TPP sensors are practical due to ease of excitation and high sensitivity, and they are particularly suitable for label-free, real-time detection in biological models (Riedel et al., 2014; Gao et al., 2014).

2. One dimensional nanostructure as sensor

In this study, a one-dimensional photonic crystal is designed, with a thin gold layer deposited on top. This structure supports TPP waves. The photonic crystal in this structure consists of 12 alternating layers of zirconium dioxide (ZrO_2) and silicon dioxide (SiO_2). The thickness of the gold layer and the reflection angle were optimized by simulations to enhance the sensor's performance. The multilayer structure was deposited on a glass substrate following a stacking sequence (LH), where "L" represents the low refractive index layer (SiO_2) and "H" represents the high refractive index layer (ZrO_2). By engineering the layers in the photonic crystal, a photonic bandgap can be created at the central wavelength λ_0. For this purpose, the thickness of each layer is determined by the formula $d = \lambda_0/4n$, where n is the refractive index of that layer at a certain wavelength. Based on the conditions of the special mode and using the transfer matrix method, assuming low optical losses ($\gamma \ll \omega$) and partial frequency separation from ω_0, the resonance frequency ω of the full mode can be approximately estimated:

$$\omega \approx \frac{\omega_0}{1 + ((2n_A\omega_0)/\sqrt{\varepsilon_b}\beta\omega_p)} \quad (1)$$

where ω_p is the metal plasma frequency, γ is the damping constant, and ε_b is the background dielectric constant. This indicates that the resonance conditions depend on the dielectric stack parameters and metal properties (Plaschke and Kopitz, 2015). In TPPs, because the field enclosed in the metal and dielectric boundary is sensitive to surface changes, this feature can be used for sensing. In fact, local refractive index changes cause measurable changes in resonance conditions. Excitation of TPPs with unpolarized light and without coupling elements makes them a powerful tool for optical sensing applications.

The photonic crystal was designed with a central wavelength of 635 nm. The multilayer structure consisted of alternating SiO_2 and ZrO_2 layers with thicknesses of 108.96 nm and 77.67 nm, respectively, following a quarter-wavelength design. The gold layer was deposited by sputtering, while the dielectric layers were fabricated using a dedicated deposition facility to ensure improved thickness accuracy and uniformity. Optical measurements were performed using an unpolarized broadband light source under normal incidence. To excite the TPP, and according to the penetration depth of gold, the gold layer thickness was chosen to be approximately 25-75 nm. In TPPs, since most of the incident light energy is transferred to the surface wave, we expect that nothing is visible in the transmission spectrum. On the other hand, in the transmission spectrum, as the gold thickness increases, the intensity of the transmitted light decreases and analysis becomes difficult. For this purpose, we simulated and analyzed the transmission and reflection spectra. According to the simulation and analysis, we reached an optimal sensor arrangement.

To optimize the angle of incidence, Essential Macleod software was used for simulation. In the simulations, light from different angles hit the sensor surface, and the reflection spectrum was recorded. By analyzing the reflection spectra, the incidence angle at which the strongest resonance occurs was identified. With this, the arrangement in which the performance of the sensor is increased was used. In fact, Simulations identified the conditions that maximize sensor accuracy and efficiency.

In order to optimize the thickness of the gold layer, a simulation was also performed with the transfer matrix method via Macleod's Essential software. After modeling the photonic crystal in the software, a layer of gold with variable thickness was placed on top of it. Reflectance and transmission spectra were recorded for different thicknesses of gold from 30 to 60 nm. For the transmission spectrum, the resonance was not observed in the transmission spectrum, and with the increase in the thickness of gold, the intensity of the transmitted light also decreased drastically. Consequently, we further focus on the reflectance spectrum. These simulations help us to get the final thickness of the gold layer, and as a result, test time and costs are reduced.

After making the sensor according to the results of the simulations, the transmission spectrum of the sensor was

measured using a UV-VIS spectrophotometer. The sensor was installed in the chamber and vertically exposed to the radiation of the broadband deuterium halogen source in the wavelength range of 200 to 900 nm. The detector collected the transmitted light, and the resulting spectrum was recorded for analysis. This step was recorded to ensure stable stimulation of the TPPs and before any biological experiments, and in the absence of cells under natural light irradiation.

The reflectance spectrum was first collected at multiple angles of incidence. In this arrangement, a broadband lamp was used in the wavelength range of 200 to 900. The aligned light hit the sample at different angles by a motorized goniometer, and the reflected light was recorded by the detector on the motorized goniometer. These measurements allow us to identify the angle at which the resonance of the TPP occurred (figure 1 d). These measurements were used to confirm the presence of TPP and archived for possible future analysis.

Cell-based sensing

All further measurements were made at the natural radiation angle. A broadband, unpolarized source was used in the wavelength range of 200 to 900 nm. The source light was delivered vertically by a reflective fiber, and the same fiber collected the reflected light and directed it to the spectrometer. This configuration allows real-time acquisition of the reflection spectrum. These initial measurements were performed prior to cell culture to characterize the optical response of the sensor and confirm successful excitation of TPPs. All measurements were repeated three times to ensure reproducibility.

Next, the sensor made in sterile conditions was transferred to Genogen's specialized laboratory. All animal care and use procedures for neural stem cell harvesting were performed according to the guidelines approved by the Institutional Animal Care and Use Committee of Tarbiat Modares University. Neural stem cells were isolated from the hippocampus and SVZ of the brain of newborn Wistar rats by enzymatic digestion with collagenase, filtering, and centrifugation. Third passage cells were seeded (2×10^5 cells/cm^2) on the gold surface of the sensor, which was covered with DMEM/F12 medium supplemented with B27 and FBS and incubated for 24 h to establish firm adhesion. Cells were cultured under these conditions prior to STZ treatment.

A natural radiation sensor arrangement was used to record data from STZ-treated neural stem cells. That is, the light is irradiated to the sample by a broadband source of 200 to 900 nm through a reflective fiber, and the reflection spectrum is directed to the spectrometer by the same fiber. For STZ treatment, following protocols reported in previous studies (Biswas et al., 2016), cells were exposed to 1 mM STZ. The first optical measurement was recorded immediately after adding STZ (0 h), and subsequent measurements were taken at 17 h and 30 h. These measurements tracked changes in the resonance wavelength and intensity of the sensor, which serve as indicators of cellular responses to STZ exposure. This sensing method allows for label-free monitoring of cellular changes. No independent biochemical or viability assays were performed in this study to directly assess cellular pathology (figure 2).

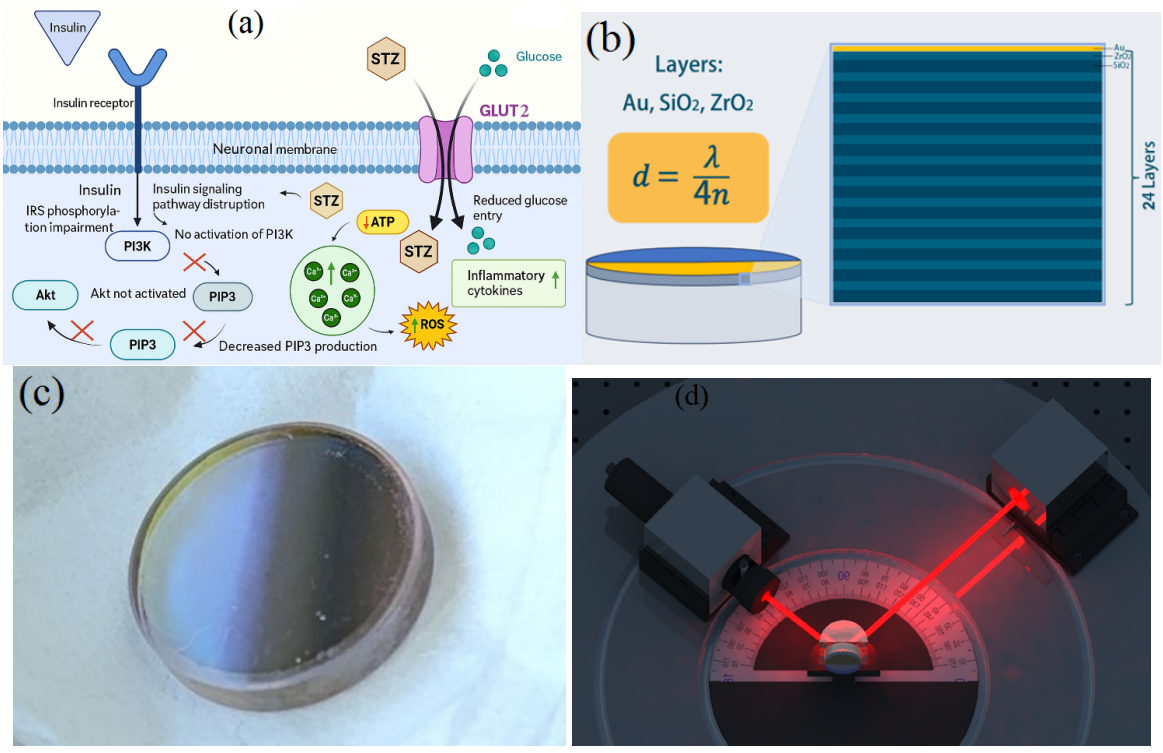

Figure 1. (a) Schematic illustration of streptozotocin (STZ)-induced disruption of insulin signaling in neurons (Crunfli et al., 2018), (b) Schematic diagram of the designed sensor architecture, showing the 1D photonic crystal composed of SiO_2 and ZrO_2 layers and a 40 nm gold layer, (c) Photograph of the fabricated TPP sensor, (d) Schematic of the angle-resolved reflectance measurement setup, including the light source in wavelength of 635 nm, cylindrical prism, TPP sensor, and detector.

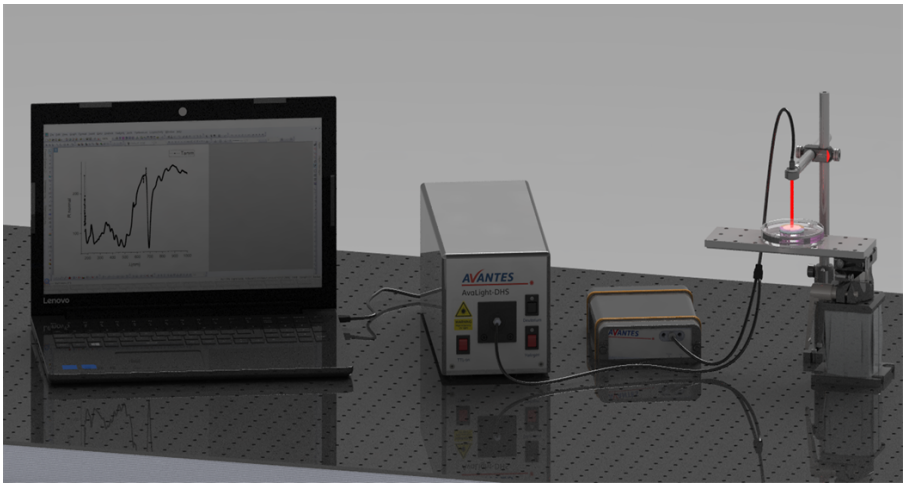

Figure 2. Schematic of the cell-based sensing setup, including the broadband light source, reflective fiber, TPP sensor, and spectromete.

3. Results and discussion

Transmission spectra were recorded for the gold layer with thicknesses of 30 to 60 nm in the sensor. With increasing gold thickness, plasmonic resonance is not visible in the transmission spectrum. The peak observed at the photonic bandgap edge is attributed to the photonic crystal structure and is not associated with TPP excitation.

As the thickness of the gold layer increases, the intensity of the transmitted light decreases. This reduction in the intensity of transmitted light is due to the increase in ohmic losses in the metal (figure 3).

Figure 4 a shows the reflection intensity at different irradiation angles on the gold-coated sensor. By decreasing the angle from 50 degrees to 0 degrees (normal radiation), the resonance slope increases, calculated at a fixed gold thickness of 30 nm. FWHM for incident angles of 50, 35, 20, and 0 are equal to 14, 12, 10, and 9 nm, respectively. In fact, the FWHM decreased from 14 to 9 nm as the angle decreased. This means that in normal incidence, the field is

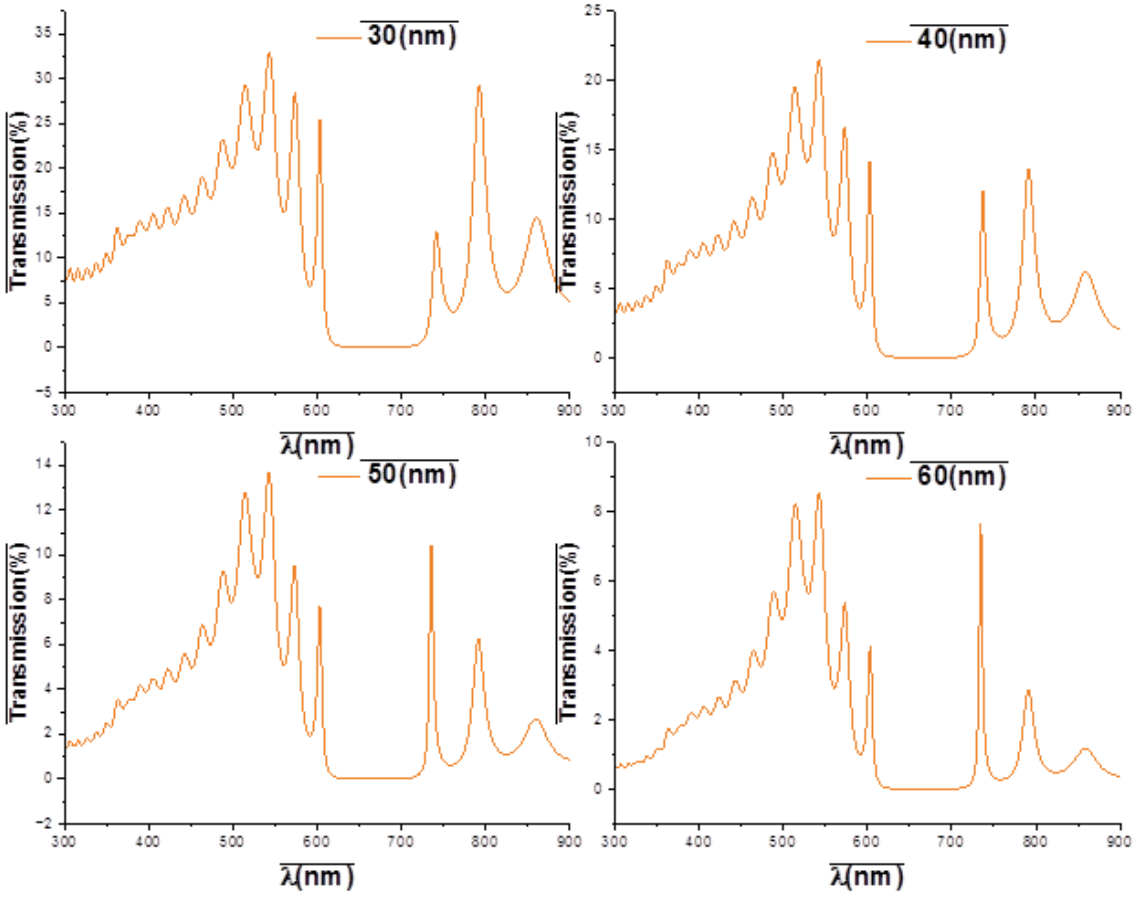

Figure 3. The calculated normal incidence transmission spectra of the TPP sensor for Au-film thicknesses of 30, 40, 50, and 60 nm.

more confined, and the efficiency of the sensor increases. According to the reflection spectrum analysis, the contrast is preserved even at higher gold thicknesses. That is, reflection-based analysis increases the stability of the sensor array against structural fluctuations, which is a major advantage in Alzheimer's sensing. Figure 4 b shows the calculated reflectance spectra for different gold thicknesses (30 to 60 nm) under normal incidence. The FWHM for gold thicknesses of 30, 40, 50, and 60 nm is 9, 5, 3, and 3 nm, respectively, which decreases from 9 to 5 nm. The deepest resonance occurs in gold with a thickness of 40 nm. As the thickness of gold increases to 50 and 60 nm, the resonance depth decreases due to the increase in metal absorption. Resonance depth is important for us to have a more stable sensor, and for this reason, 40 nm thickness was chosen as the thickness of gold in the sensor.

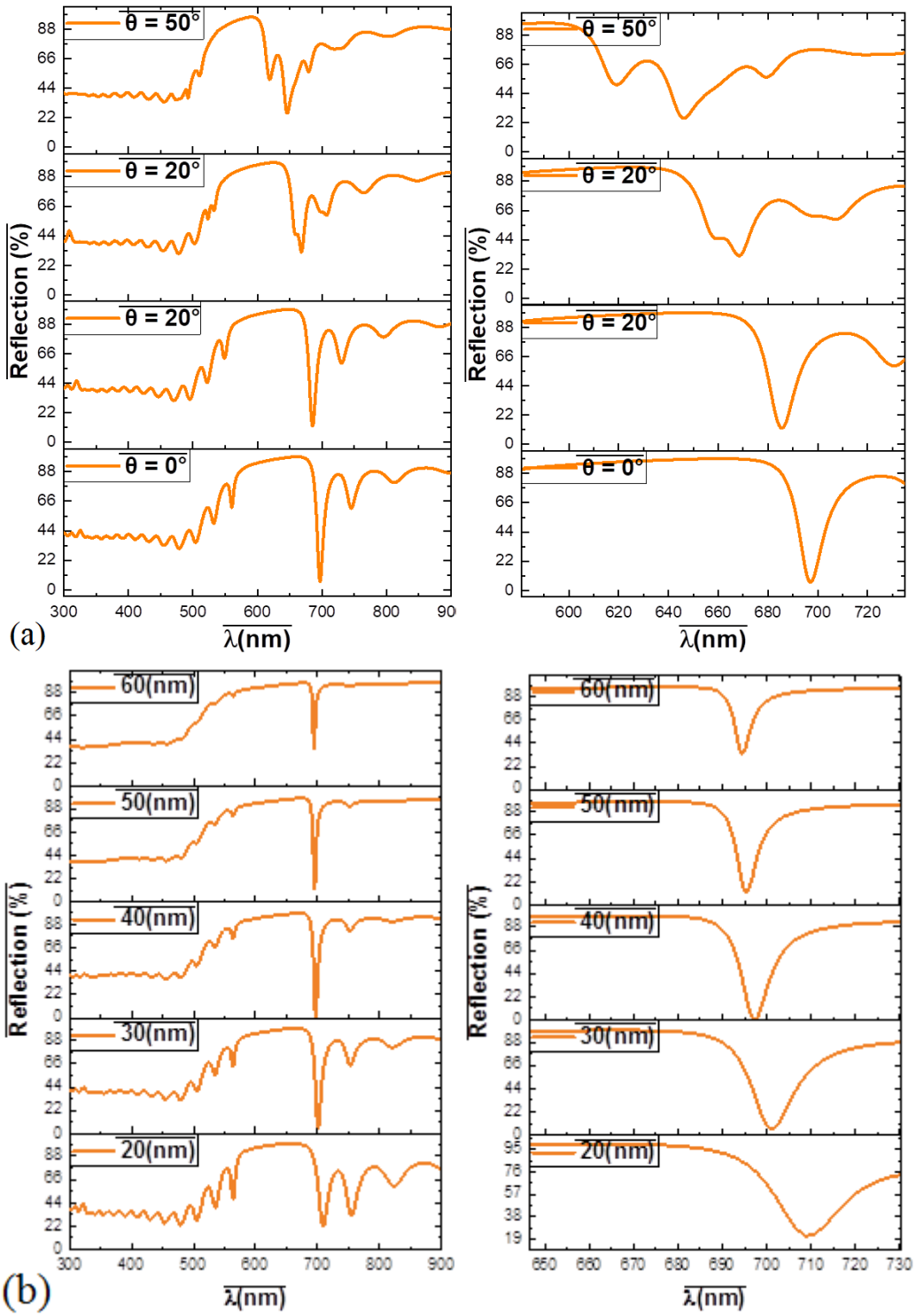

Figure 4. (a) Effect of incident angle on the sensor reflection: as the angle decreases from 50° to normal incidence, the resonance dip sharpens (FWHM: 14→9 nm) and the reflectance minimum deepens. (b) Calculated normal incidence reflectance spectra for Au-film thicknesses of 20–60 nm, showing sharpening of the resonance dip (FWHM: 9→5 nm) and deepest minimum at 40 nm Au thickness.

After optimization, the full width at half maximum (FWHM) was reduced from 14 nm to 5 nm. Accordingly, the figure of merit (FOM), which is inversely proportional to FWHM, is improved from FOM $\propto 1/14 \approx 0.069$ to FOM $\propto 1/5 \approx 0.19$.

UV-VIS transmission spectra were recorded for the photonic crystal without gold and the photonic crystal with a 40 nm gold layer. The results show that the transmission intensity in the structure with a gold layer decrease significantly. As we expected, there is no resonance associated with TPP in the spectrum. These results show why transmission was not used for the sensor arrangement (figure 5 a). To make sure that the surface state is completely excited in the reflection spectrum and to characterize the sensor, we recorded the reflection spectrum from the cell-free sensor at different radiation angles and normal radiation. In the reflection spectrum, a dip appears at 60 degrees, which corresponds to the resonance angle of the TPP. This confirms that the TPP has been successfully executed (figure 5 b).

Figure 5 c is the intensity of reflection in terms of wavelength in normal incidence. A dip is observed at the wavelength of 698 nm, which is attributed to the TPP mode. This value is consistent with the simulation results. This finding assures us that we are ready for the next steps of the experiment and that the surface state is exciting. On the other hand, this spectrum represents the baseline response of the sensor before cell culture.

An optical microscope was used to see the morphology of neural stem cells cultured on the sensor surface. As shown in Figure 5 d there are elongated and interconnected structures on the sensor, indicating that the cells are well attached to the sensor. This confirms that the photonic sensor is biocompatible and that cells can grow on it. This cell adhesion is advantageous for sensing applications because the changes in the nerve cells and the refractive index around them can lead to measurable changes in the TPP.

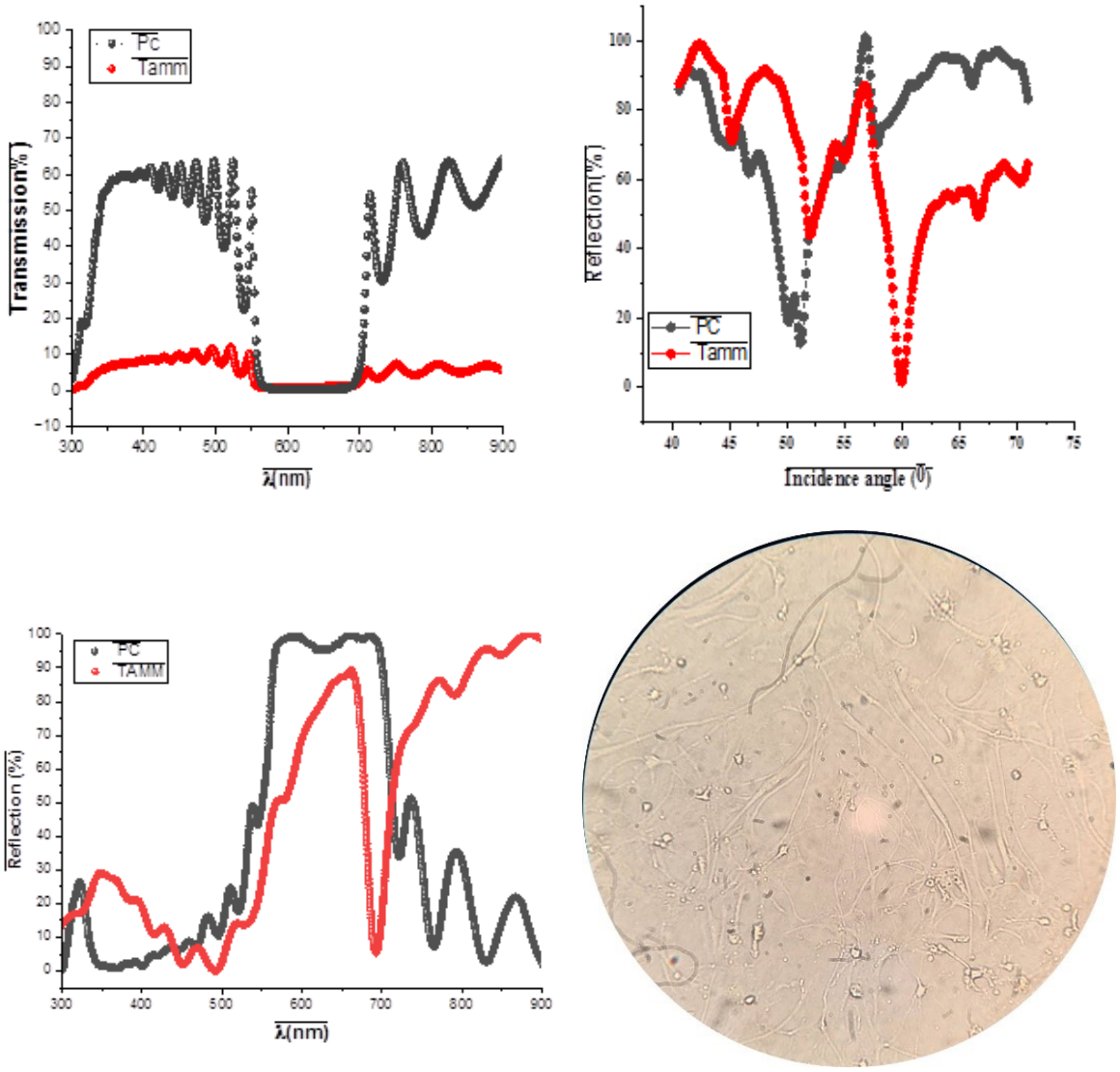

Figure 5. (a) UV-Vis transmission spectra of the 1D photonic crystal sensor. (b) Angle-resolved TM and TE reflectance of the bare sensor $\theta = 40 - 75°$, showing a pronounced dip at $\theta = 60°$ corresponding to Tamm wave coupling. (c) Normal incidence reflectance spectrum displaying the TPP dip at 698 nm, consistent with simulations. (d) Microscopic image of neural stem cells cultured directly on the TPP sensor surface.

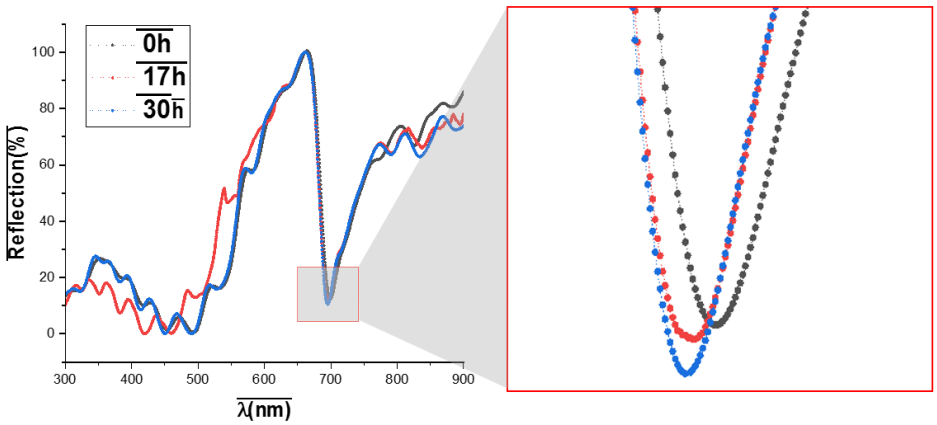

Figure 6. Normal incidence reflectance spectra showing progressive blue shift of the TPP resonance following STZ treatment at 0, 17, and 30 h.

Cell-based sensing results

After confirming the resonance of the TPP and cell growth on the sensor substrate, we added STZ to the cell culture medium. STZ causes Alzheimer's-like changes in nerve cells, which lead to oxidative stress in nerve cells, amyloid-beta accumulation, and hyperphosphorylated tau. Due to the high sensitivity of the sensor, changes in the surface of the cells will appear as changes in the refractive index of the environment and as a result, changes in the resonance wavelength of the TPP.

The reflection spectrum under normal incidence was recorded at 0, 17, and 30 h following STZ exposure. The resonance wavelength exhibited a gradual blue shift from 699.5 nm at 0 h to 696.5 nm and 695.5 nm at 17 h and 30 h, respectively. All measurements were performed in triplicate ($n = 3$), and the data are presented as mean $\pm$ standard deviation. Due to the limited number of time points, no quantitative kinetic analysis is claimed. The observed blue shift and increased depth of the reflection minimum indicate a measurable optical response of the TPP resonance to STZ-induced cellular changes (figure 6).

Figure 7 shows the time evolution of the resonance wavelength ($\Delta\lambda$). The resonance changes show an apparent exponential-like trend, which indicates the progressive changes in the refractive index caused by cellular responses to STZ addition. The decay profile was fitted using a monoexponential function to phenomenologically describe the temporal response. Yielding an estimated characteristic time constant on the order of ~ 21 h. This behavior shows that cellular changes after STZ addition occur most rapidly during the first hours after treatment and gradually slow down at later time points. These findings confirm that the TPP assay provides a highly sensitive, label-free sensing method capable of real-time monitoring of dynamic cellular responses associated with Alzheimer's-like cellular responses.

4. Conclusion

In this study, we investigated and evaluated the feasibility of a TPP optical biosensor for label-free detection of STZ-induced Alzheimer-like cellular changes in cultured neural stem cells. Through transfer matrix simulations and experimental reflectometry, we identified a sensor geometry with a 40 nm gold film on it that provides a narrow TPP resonance and high contrast in the visible range. The resonance wavelength of the sensor changes exponential-like with STZ exposure time, showing high sensitivity consistent with changes in the cell surface refractive index. Observed optical shifts were qualitatively correlated with STZ-induced cellular responses, suggesting the potential of TPP-based photonic crystals to monitor Alzheimer-like cellular responses in vitro and to enable

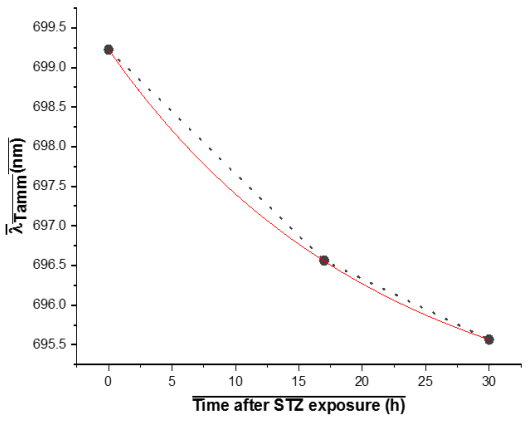

Model	ExpDec1
Equation	y = A1*exp(-x/t1) + y0
Plot	Book1_B
y0	694.40353 ± 0
A1	4.82267 ± 0
t1	21.0568 ± 0
Reduced Chi-Sqr	0
R-Square (COD)	0.99999
Adj. R-Square	0

Figure 7. Temporal evolution of the TPP resonance wavelength ($\Delta\lambda$) under STZ treatment, displaying an apparent exponential-like blue shift over 0–30 h.

development of compact and integrated optical devices for cellular sensing; however, the limited number of time points and absence of independent biochemical or viability assays restrict quantitative interpretation. Future studies will focus on optimizing surface chemistry, microfluidic integration, and multiplex detection of additional biomarkers.

Authors contributions
Authors have contributed equally in preparing and writing the manuscript.

Availability of data and materials
The data that support the findings of this study are available from the corresponding author, upon reasonable request.

Conflict of interests
The authors declare that they have no known competing financial interests or personal relationships that could have appeared to influence the work reported in this paper.

References

Ahmad S., Aijaz M., Ahmad M., Hafeez A., Asif M., Kumar A., Al-Taie A., Ansari M. A. (2023) Early Detection of Alzheimer's disease by using the Latest Techniques. *Authorea Preprints*

Bessonov V. O., Afinogenov B. I., Popkova A., Fedyanin A. A. (2017) Femtosecond relaxation dynamics of Tamm plasmon-polaritons (Conference Presentation). In Ultrafast Phenomena and Nanophotonics XXI. *SPIE* 10102:54–54.

Bikbaev R. G., Pykhtin D., Vetrov S. Y., Timofeev I. V., Shabanov V. F. (2021) Model of the Tamm plasmon polariton based solar cell. arXiv preprint arXiv:2109.14475

Biswas J., Goswami P., Gupta S., Joshi N., Nath C., Singh S. (2016) Streptozotocin induced neurotoxicity involves Alzheimer's related pathological markers: a study on N2A cells. *Molecular Neurobiology* 53:2794–2806.

Chang C. Y., Chen Y. H., Tsai Y. L., Kuo H. C., Chen K. P. (2014) Tunability and optimization of coupling efficiency in Tamm plasmon modes. *IEEE Journal of Selected Topics in Quantum Electronics* 21:262–267.

Chen K. P. (2020) Application and developments in Tamm plasmonics polaritons. In Plasmonics: Design, Materials, Fabrication, Characterization, and Applications XVIII. *SPIE* 11462:114621G.

Chen W., Long K. D., Lu M., Chaudhery V., Yu H., Choi J. S., Polans J., Zhuo Y., Harley B. A., Cunningham B. T. (2013) Photonic crystal enhanced microscopy for imaging of live cell adhesion. *Analyst* 138:5886–5894.

Crunfli F., Mazucanti C. H., de Moraes R. C. M., Costa A. P., Rodrigues A. C., Scavone C., Torrao A. D. S. (2018) NO-dependent Akt inactivation by S-nitrosylation as a possible mechanism of STZ-induced neuronal insulin resistance. *Journal Of Alzheimer's Disease* 65:1427–1443.

Danz N., Sinibaldi A., Michelotti F., Descrovi E., Munzert P., Schulz U., Sonntag F. (2012) Improving the sensitivity of optical biosensors by means of Bloch surface waves. *Biomedical Engineering/Biomedizinische Technik* 57:584–587.

Das D., Boyer P., Salvi J. (2021) Refractive index sensor based on a Tamm Fabry–Perot hybrid resonance. *Applied optics* 60:4738–4745.

Du B., Li Y., Yang D., Lu H. (2019) High-performance optical sensing based on electromagnetically induced transparency-like effect in Tamm plasmon multilayer structures. *Applied Optics* 58:4569–4574.

Elsheikh S., Coles N. P., Achadu O. J., Filippou P. S., Khundakar A. A. (2024) Advancing brain research through surface-enhanced raman spectroscopy (SERS): current applications and future prospects. *Biosensors* 14:33.

Gao Y., Gan Q., Bartoli F. J. (2014) Breakthroughs in photonics 2013: research highlights on biosensors based on plasmonic nanostructures. *IEEE Photonics Journal* 6:1–5.

Gheorghiu M., David S., Polonschii C., Olaru A., Gaspar S., Bajenaru O., Popescu B. O., Gheorghiu E. (2014) Label free sensing platform for amyloid fibrils effect on living cells. *Biosensors and Bioelectronics* 52:89–97.

Gong Y., Liu X., Wang L., Lu H., Wang G. (2011) Multiple responses of TPP-assisted near-perfect absorption in metal/Fibonacci quasiperiodic photonic crystal. *Optics Express* 19 (10): 9759–9769.

Gryga M., Ciprian D., Hlubina P. (2020) Bloch surface wave resonance based sensors as an alternative to surface plasmon resonance sensors. *Sensors* 20:5119.

Gu Y., Bi X., Ye J. (2020) Gap-enhanced resonance Raman tags for live-cell imaging. *Journal of Materials Chemistry B* 8:6944–6955.

Gupta D., Nair R. V. (2015) Optical surface states at the interface between a metal and dielectric nanophotonic structure. *IEEE. Workshop on Recent Advances in Photonics (WRAP),* 1–4.

Haidar O., Mathmann B., Dusch Y., El Barghouti M., Lévêque G., Akjouj A., Mir A., Talbi A. (2024) The improvement of Tamm interface state detection by using a porous layer between a metal nanostructured grating and a DBR. *MDPI* 97:136.

Homola J., Piliarik M. (2006) Surface plasmon resonance (SPR) sensors. In Surface plasmon resonance based sensors. Springer Berlin Heidelberg:45–67.

Hsiao W. W. W., Angela S., Le T. N., Ku C. C., Hu P. S., Chiang W. H. (2023) Evolution of detecting early onset of alzheimer's disease: from neuroimaging to optical immunoassays. *Journal of Alzheimer's Disease* 93:821–845.

Huang S. G., Chen K. P., Jeng S. C. (2017) Phase sensitive sensor on Tamm plasmon devices. *Optical Materials Express* 7:1267–1273.

Kaliteevski M., Iorsh I., Brand S., Abram R. A., Chamberlain J. M., Kavokin A. V., Shelykh I. A. (2007) Tamm plasmon-polaritons: Possible electromagnetic states at the interface of a metal and a dielectric Bragg mirror. *Physical Review B—Condensed Matter and Materials Physics* 76:165415.

Kavokin A. V., Shelykh I. A., Malpuech G. (2005) Lossless interface modes at the boundary between two periodic dielectric structures. *Physical Review B—Condensed Matter and Materials Physics* 72:233102.

Konopsky V. N., Alieva E. V. (2007) Photonic crystal surface waves for optical biosensors. *Analytical Chemistry* 79:4729–4735.

Kulichikhin K. Y., Fedotov S. A., Rubel M. S., Zalutskaya N. M., Zobnina A. E., Malikova O. A., Neznanov N. G., Chernoff Y. O., Rubel A. A. (2021) Development of molecular tools for diagnosis of Alzheimer's disease that are based on detection of amyloidogenic proteins. *Prion* 15:56–69.

Lathuiliere A., Jo Y., Perbet R., Donahue C., Commins C., Quittot N., Fan Z., Bennett R. E., Hyman B. T. (2023) Specific detection of tau seeding activity in Alzheimer's disease using rationally designed biosensor cells. *Molecular Neurodegeneration* 18:53.

Lee K. J., Wu J. W., Kim K. (2013) Enhanced nonlinear optical effects due to the excitation of optical Tamm plasmon polaritons in one-dimensional photonic crystal structures. *Optics Express* 21:28817–28823.

Lei H. (2010) Amyloid and Alzheimer's disease. *Protein & Cell* 1 (4): 312.

Li Q., Chen Z., Zhang Y., Ding S., Ding H., Wang L., Xie Z., et al. (2023) Imaging cellular forces with photonic crystals. *Nature Communications* 14:7369.

Maier S. A. (2007) Plasmonics: fundamentals and applications. New York: Springer:45.

Morozov G. V., Sprung D. W. L., Martorell J. (2006) Surface EM waves on 1D photonic crystals. In Photonics North. *SPIE* 6343:506–515.

Normani S., Carboni F. F., Lanzani G., Scotognella F., Paternò G. M. (2022) The impact of Tamm plasmons on photonic crystals technology. *Physica B: Condensed Matter* 645:414253.

Orojloo M. H., Jabbari M., Solooki Nejad G., Sohrabi F. (2024) Multi-channel graphene-based perfect absorbers utilizing Tamm plasmon and Fabry-Perot resonances. *Optics Express* 32

Park J. S., Kim S. T., Kim S. Y., Jo M. G., Choi M. J., Kim M. O. (2019) A novel kit for early diagnosis of Alzheimer's disease using a fluorescent nanoparticle imaging. *Scientific Reports* 9:13184.

Paula V. D. J. R. D., Guimarães F. M., Diniz B. S., Forlenza O. V. (2009) Neurobiological pathways to Alzheimer's disease: Amyloid-beta, TAU protein or both? *Dementia & Neuropsychologia* 3:188–194.

Plaschke K., Kopitz J. (2015) *In vitro* streptozotocin model for modeling Alzheimer-like changes: effect on amyloid precursor protein secretases and glycogen synthase kinase-3. *Journal of Neural Transmission* 122:551–557.

Polo Jr J. A., Lakhtakia A. (2011) Surface electromagnetic waves: a review. *Laser & Photonics Reviews* 5:234–246.

Pykhtin D. A., Bikbaev R. G., Timofeev I. V., Vetrov S. Y., Shabanov V. F. (2024) Perovskite-based solar cell in tamm plasmon-polariton structure. *Doklady Rossijskoj akademii nauk. Fizika, Tehničeskie Nauki* 514:29–33.

Riedel T., Majek P., Rodriguez-Emmenegger C., Brynda E. (2014) Surface plasmon resonance: advances of label-free approaches in the analysis of biological samples. *Bioanalysis* 6:3325–3336.

Rong G., Sawan M. (2023) Tamm Plasmon Polariton Biosensors Based on Porous Silicon: Design, Validation and Analysis. *Biosensors* 13:1026.

Sasin M. E., Seisyan R. P., Kalitteevski M. A., Brand S., Abram R. A., Chamberlain J. M., Egorov A. Y., Vasil'Ev A. P., Mikhrin V. S., Kavokin A. V. (2008) Tamm plasmon polaritons: Slow and spatially compact light. *Applied Physics Letters* 92

Schlachetzki J., Saliba S. W., Oliveira A. C. P. D. (2013) Studying neurodegenerative diseases in culture models. *Brazilian Journal of Psychiatry* 35:S92–S100.

Serrano-Pozo A., Frosch M. P., Masliah E., Hyman B. T. (2011) Neuropathological alterations in Alzheimer disease. *Cold Spring Harbor Perspectives in Medicine* 1 (1): 006189.

Singh A. K., Mittal S., Das M., Saharia A., Tiwari M. (2023) Optical biosensors: A decade in review. *Alexandria Engineering Journal* 67:673–691.

Sinibaldi A., Danz N., Descrovi E., Munzert P., Schulz U., Sonntag F., Dominici L., Michelotti F. (2012) Direct comparison of the performance of Bloch surface wave and surface plasmon polariton sensors. *Sensors and Actuators B: Chemical* 174:292–298.

Su M., Li K., Wang C., Wu L., Yang S., Lin Q., Li Y., Tang L., Zhou R. (2023) Tamm-plasmon-polariton biosensor based on one-dimensional topological photonic crystal. *Results in Physics* 48:106454.

Tamm I. (1932) On the possible bound states of electrons on a crystal surface. *Phys. Z. Sowjetunion* 1:733–735.

Xue C. H., Wu F., Jiang H. T., Li Y., Zhang Y. W., Chen H. (2016) Wide-angle spectrally selective perfect absorber by utilizing dispersionless Tamm plasmon polaritons. *Scientific Reports* 6:39418.

Zeidan E., Kepley C. L., Sayes C., Sandros M. G. (2015) Surface plasmon resonance: a label-free tool for cellular analysis. *Nanomedicine* 10:1833–1846.